Effect of Polymer Charge and Geometrical Confinement on Ion Distribution and the Structuring in Semidilute Polyelectrolyte Solutions: Comparison between AFM and SAXS

Dan Qu,*,† Jan S. Pedersen,‡ Sébastien Garnier,§ André Laschewsky,§ Helmuth Möhwald,† and Regine v. Klitzing⊥

Max-Planck-Institute of Colloids and Interfaces, Am Mühlenberg 1, 14476 Golm, Germany; Department of Chemistry, University of Aarhus, Langelandsgade 140, DK-8000 Aarhus c, Denmark; Frauhofer Institute for Applied Polymer Research, Geiselbergstr. 69, 14476 Golm, Germany; and Stranski-Laboratory for Physical and Theoretical Chemistry, Technical University of Berlin, Strasse des 17. Juni 124, D-10623 Berlin, Germany

Received December 14, 2005; Revised Manuscript Received July 7, 2006

ABSTRACT: This paper focuses on the effect of geometrical confinement on the structruring of a semidilute polyelectrolyte solution in a thin film geometry. Studying poly-*N*-[tris(hydroxymethyl)methyl]acrylamide-*co*-2-acrylamido-2-methylpropanesulfonate (PTRIS-*co*-AMPS) with different degrees of charge allows a deeper insight into the ion distribution around the polymer chains. Results from atomic force microscopy (AFM) force−distance measurements in films are compared with results from small-angle X-ray scattering (SAXS) in bulk. It is found that the characteristic lengths obtained from force oscillation measured by AFM, such as the intermediate chain distance (mesh size) and the correlation length, correlate well with those obtained from the structure peak measured by SAXS. In the direction perpendicular to the film surface, both length scales of the meshlike structure, i.e., the average chain distance and the correlation length, are not influenced by the geometrical confinement. The dependencies of force period and decay length on the polymer charge are analyzed in detail and related to the counterion distribution in the solutions. A new model for counterion condensation is proposed, in which the condensed ions are not fixed on the polyion chains and can exchange freely with the free ions. However, there is still a length scale beyond which the ion condensation theory of Manning and Oosawa is valid. Results from conductivity measurements support the proposed model.

I. Introduction

Polyelectrolytes are polymer chains that contain ionizable groups. When dissolved in water, these ionizable groups dissociate and the chains become charged while releasing counterions into the solution. A large number of biological macromolecules such as DNA and most proteins and synthetic macromolecules belong to this category. Since polyelectrolytes have higher solubility in water than neutral polymers and possess interesting properties in solutions due to their ionizability, they are widely used in industry, e.g., as flocculation agents in paper making and wastewater treatment, or in the coating of various materials such as paper, textile, and contact lenses. The conformation of the polyelectrolyte chains and the ion distribution are strongly related to each other and determine the macroscopic properties (e.g., rheology) of the system. Because of an enhanced interest in miniaturization, motivated by applications in nanotechnology, their behaviors in thin films have come more and more into research focus.

One main scientific interest in polyelectrolytes is the chain conformation in solutions, which depends critically on the concentration. In the so-called semidilute regime above certain threshold concentration, the polyelectrolyte chains are assumed to overlap and to form a transient network structure.[1] The theoretical mesh size ξ scales with the concentration c of the repeat unit as $c^{-1/2}$. In the following years, this theory was further developed in two directions: the Odijk−Skolnick−Fixman (OSF) model[2,3] for strongly charged chains and the model of Dobrynin et al.[4] for weakly charged, flexible chains. The theoretical predictions are verified by experimental studies. For instance, the small-angle scattering (SANS or SAXS) spectra of polyelectrolyte solutions show structure peaks, indicating intermolecular interactions within the solutions. The peak position q_{max} scales with $c^{1/2}$ in bulk solutions.[5−11] Under the assumption that the Bragg relation is justified, a length can be calculated by $2\pi/q_{max}$, which corresponds to the mesh size ξ (i.e., the average chain distance), thus confirming the theoretical prediction: $\xi \sim c^{-1/2}$.

To study the effect of geometrical confinement of polyelectrolyte solutions in thin films, thin film pressure balance (TFPB)[11−17] and atomic force microscopy (AFM)[18−22] techniques were used. Both the disjoining pressure across the film in TFPB experiments and the force in AFM experiments oscillate during approach of the interfaces. In semidilute regime, the oscillation period also scales with $c^{-1/2}$. Further studies combined small-angle scattering and TFPB techniques[11,23,24] in order to determine the effect of thin film confinement on the mesh structure. It was found that the oscillation period is equal to the mesh size of the respective bulk solution, suggesting no effect of thin film confinement. However, as negative pressure as well as the mechanically unstable part cannot be obtained with the TFPB technique, it is difficult to analyze further the partial pressure vs film thickness curves. AFM has the advantage of obtaining almost complete oscillatory force curves, which can be fitted to the form of a harmonic oscillation with an envelope of exponential decay. Such quantitative analysis yields

† Max-Planck-Institute of Colloids and Interfaces.
‡ University of Aarhus.
§ Frauhofer Institute for Applied Polymer Research.
⊥ Technical University of Berlin.
* Corresponding author. E-mail: dan.qu@mpikg-golm.mpg.de.

10.1021/ma052676q CCC: $33.50
Published on Web 09/16/2006

detailed information on not only the mesh structure but also the interactions within the system.[21] Therefore, to achieve better comparison between the bulk solution and the film, it is necessary to combine the AFM and the small-angle scattering techniques and perform a more thorough analysis of both.

The structuring of polyelectrolyte in solutions also depends crucially on the charge dissociation and counterion distribution. The effect of different charge fraction of polyelectrolyte chains with hydrophilic[11,12,14,15] and hydrophobic[12,21,24] backbones has been studied. The scaling behavior of the mesh size ξ vs c is a critical test of the structure, with $\xi \sim c^{-1/2}$ indicating a mesh structure while $c^{-1/3}$ indicating the dominance of microdomains.[1,4] For those with hydrophobic backbones, the effect of backbone hydrophobicity competes with the effect of charge to determine the chain structuring. With decreasing degree of charge, the influence of the backbone hydrophobicity becomes more dominant, leading to a transition of the scaling behavior of the mesh size ξ from $c^{-1/2}$ to $c^{-1/3}$,[21,25] indicating a gradual formation of microdomains. Such formation of microdomains is subdued in the case of polyelectrolyte with hydrophilic backbones, where the scaling law of $\xi \sim c^{-1/2}$ remains unchanged. It is thus suitable to use a hydrophilic polyelectrolyte for studying the correlation of structuring and ion distribution. According to the theory of Manning and Oosawa which was based on a simple model of a rodlike, single chain, when the average distance between two charges on a polyelectrolyte chain is smaller than the Bjerrum length l_B ($l_B \approx 7$ Å in water at room temperature), the effective charge will be renormalized such that the average distance between two charges on the chains becomes equal to the Bjerrum length.[26−28] However, polyelectrolyte chains are entangled in semidilute solutions, far from the rod−chain assumption of the Manning−Oosawa model. Several experiments[9,15] in semidilute polyelectrolyte solutions show that the average chain distance of the mesh structure remains unchanged above the threshold charge fraction predicted by Manning's theory. On the other hand, there are many examples where polyelectrolyte systems do not follow the Manning model.[29−33] In addition, certain molecular simulations showed that condensed ions also have certain mobility and will move along the chains in even very weak electric field.[34,35] This indicates the difficulty to classify the ions in strict terms of "*free*" and "*condensed*" ions. Therefore, questions arise as to how counterions condense in semidilute polyelectrolyte solutions and how this influences the structuring of the solution. Further, film confinement may also influence the ion distribution and consequently the network structuring.

The present paper deals with the questions of how ions are distributed in a semidilute solution of hydrophilic polyelectrolyte, how this distribution influences the structuring of the network, and how a geometrical confinement affects both. A random copolymer with different charge fractions both above and below the Manning condensation threshold is chosen as the model polyelectrolyte. In comparison to many other polyelectrolytes like polystyrenesulfonate, the backbone is quite hydrophilic. AFM results in film are compared with SAXS results in bulk. The applicability of Manning's theory of ion condensation is examined for this system, and a new model is proposed for the counterion distribution in the network. Conductivity measurements were also carried out, and the results support the proposed picture of counterion condensation.

II. Experiments

II.1. Materials. Our model polyelectrolyte is poly-*N*-[tris(hydroxymethyl)methyl]acrylamide-*co*-2-acrylamido-2-methylpropanesulfonate (PTRIS-*co*-AMPS) of various nominal charge fractions *f*, whose chemical structure is shown in Figure 1. The copolymers were prepared by aqueous free radical polymerization of given mixtures of *N*-[tris(hydroxymethyl)methyl]acrylamide (TRIS) and 2-acrylamido-2-methylpropanesulfonate (AMPS) at 60 °C for 15 h, using azobis(cyanoisovalerianic acid) as initiator, as described before.[36] According to ^{1}H NMR, the copolymers are free of any residual monomer. As the copolymer composition corresponds within the analytical precision to the composition of the monomer feed even at low-to-moderate conversions, the reactivity parameters of both monomers must be close to 1. Therefore, the resulting copolymers are true random copolymers with a Bernouillian distribution of the anionic repeat units derived from AMPS along the polymer chain. As the polyelectrolyte chains stick to the column of the GPC, it is unable to determine the molecular weight. However, previous studies have shown that molecular weight has no influence on the mesh size of the mesh structure.[1−4,11,14,18,20,24,37] For vinylic polymers such as PTRIS-*co*-AMPS, the length of the repeat unit along the chain backbone is around 2.5 Å. Thus, the calculated charge fraction for Manning condensation is 36%.[9] Above this charge fraction, counterions shall condense to the chains if Manning's law is valid. Detailed osmotic pressure and SAXS measurements indicate the actual limit of the ion condensation to be around 45%.[37] With the knowledge that Manning's theory is based on a very simple model and has limitations, we still use the concept of effective charge fraction f_{eff} for convenience and use $f = 45\%$ as a rough estimation of the threshold charge fraction. The details of the limitations will be discussed later.

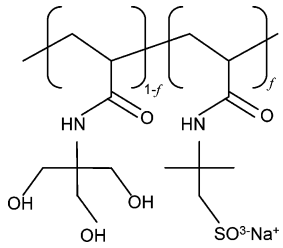

Figure 1. Chemical structure of poly-*N*-[tris(hydroxymethyl)methyl]-acrylamide-*co*-2-acrylamido-2-methylpropanesulfonate (PTRIS-*co*-AMPS) with nominal charge fraction *f*.

The AFM and conductivity experiments were performed on our sample solutions with varying charge fraction f (= 100, 80, 60, 40, 30, 20, and 10%) and repeat unit concentration c (= 0.005, 0.01, 0.02, 0.04, 0.08, and 0.1 M). The SAXS experiments were performed on only two selected series of the above sample solutions. Sample series I contains PAMPS of fixed charge fraction (f = 100%), with varying c. Sample series II contains PTRIS-*co*-AMPS of fixed repeat unit concentration (c = 0.04 M), with varying f.

II.2. Methods. II.2.1. Colloidal Probe AFM. The colloidal probe technique was first developed by Ducker et al.[38] In our experiments, a silica particle is glued with epoxy to a tipless cantilever (Ultrasharp Contact Silicon Cantilevers, CSC12) produced by μMasch. The silica particles are produced by the Bangs Laboratories, Inc., and all have a radius R of about 3.35 μm. The tip is cleaned with plasma cleaning for 10 min right before each measurement cycle to remove all the organic components on its surface. The substrate used is a silicon wafer with a native SiO_2 top layer, cleaned with the RCA method,[39] and stored in Millipore water before usage. Just before each experiment, the substrate is taken out of the water and dried in a nitrogen stream. Then a drop of the polymer solution is put onto the substrate, and the probing head is immersed in the solution. Force vs distance ($F(x)$) curves were measured with a commercial atomic force microscope MFP (Molecular Force Probe) produced by Asylum Research, Inc., and distributed by Atomic Force (Mannheim, Germany). Since the distance between the colloidal probe and the substrate is much smaller compared to the diameter of the probe, by the Derjaguin approximation, the curved surface of the silica particle can be considered as a flat surface, and the interaction energy per area $E(x)$ can be acquired from the force $F(x)$, $E(x) = F(x)/2\pi R$. As

both the polymer chains and the SiO_2 surfaces are negatively charged, there is generally no adsorption of polymer onto the surfaces. For each solution, altogether 10−20 force−distance curves were measured at different lateral positions on the same substrate as well as on different substrates to ensure reproducibility and to get good statistics. Oscillatory force curves occur, and they are fitted by the following equation:

$$\frac{F(x)}{2\pi R} = Ae^{-x/\lambda}\cos(2\pi x/d + \text{phase shift}) + \text{offset} \qquad (1)$$

where $F(x)$ is the force, R is the radius of the colloidal probe, and x is the distance between the substrate and the probe, i.e., the thickness of the liquid film between the two solid surfaces. The three important parameters that characterize the oscillation are the amplitude A, the decay length λ, and the period d. In the discussion that follows, the phase shift and offset are omitted for the sake of clarity. In fitting the force data, we have neglected the region close to hard contact, since additional nonstructural forces are contributing there. The final result of each parameter is the average of 10−20 fitting results, and the error bars are from the standard deviation.

II.2.2. Small-Angle X-ray Scattering (SAXS). The SAXS measurements were carried out on a modified version of a commercially available small-angle X-ray equipment (NanoStar), which is produced by Anton Paar, Graz, and distributed by Bruker AXS.[40] The instrument consists of a powerful rotating anode X-ray source (Cu Kα, 0.3 × 0.3 mm^2 source point, 6 kW power) and a pinhole camera with two Göbel mirrors for monochromatizing and focusing the beam. The data were collected with a two-dimensional position-sensitive gas detector (HiSTAR). The water background was subtracted and the data were converted to absolute scale using the scattering from water as a primary standard.

$$I(q) = \frac{I_1}{(q - q_{max})^2 + (\Delta q/2)^2} + I_0 \qquad (2)$$

where I_0 is the incoherent background, I_1 is the incident beam intensity, q_{max} is the peak position, and Δq is the full width at half-maximum of the peak. Δq, q_{max}, I_0, and I_1 are all obtained by fitting the data in the region of the peak. The error bars are calculated from the propagation of the standard deviation from the fits.

II.2.3. Conductivity. A commercial conductimeter WTW inoLab pH/con. Level 1 with the probe head WTW TetraCon 325 was used. The output voltage is 200 mV dc, under which the voltage drop along the contour length of each polymer chain is only on the order of microvolts. Consequently, the energy that counterions could gain from this applied voltage is much lower than the thermal energy 25 meV and could not affect the ion distribution in the solution. The conductivity κ was measured and plotted vs the repeat unit concentration c for the differently charged PTRIS-*co*-AMPS solutions.

III. Results and Discussion

Figure 2 shows some examples of the AFM force−distance oscillation curves at different repeat unit concentration c and charge fraction f. The data shows a harmonic oscillation with an exponential decay. At first glance, when c or f decreases, the amplitude decreases and the period increases. For a quantitative and systematical study, we have fitted each individual force−distance curve to eq 1.The fitted curves are also shown in Figure 2.

Figure 3 shows all the SAXS scattering data of sample series I and II, with fitted curves by the Lorenzian described in eq 2. With increasing polymer concentration, the peak shifts to higher q values. But as the charge fraction increases, the peak first shifts to higher q values and then remains at the same q-position for $f \geq 60\%$. The intensity of the scattering curves for $f = 10\%$ and $f = 20\%$ are exceptionally high due to unknown reasons. However, it should not be due to any aggregation, since the solutions are still clear. The possibility of any formation of microdomains can also be ruled out due to the strict $q_{max} \sim c^{1/2}$ dependency (as will be shown in section III.1).

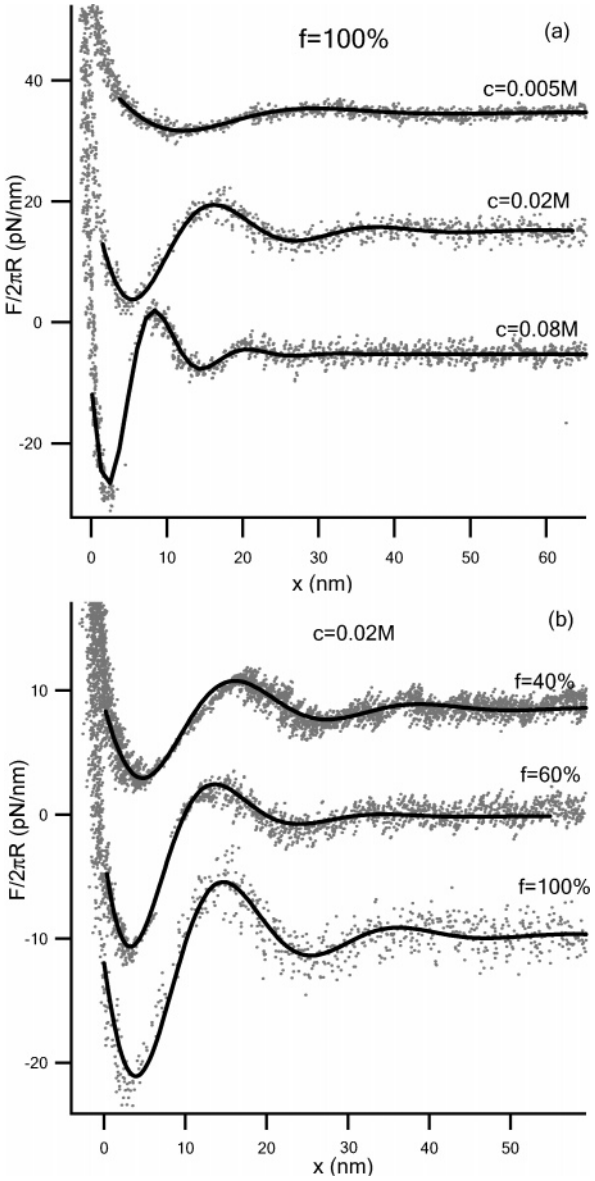

Figure 2. AFM force vs distance curves for PTRIS-*co*-AMPS (a) of different repeat unit concentration at the same charge percentage $f = 100\%$ and (b) of different charge percentages at the same concentrations $c = 0.02$ M. For better viewing, the curves are offset. Data points are fitted to the form $F/2\pi R = Ae^{-x/\lambda}\cos(2\pi x/d + \text{phase shift}) + \text{offset}$.

The validity of using the Lorenzian form for the fit is based on the assumption that there is a periodic correlation which decays exponentially, following $e^{-r/(2/\Delta q)}$, where the decay length $2/\Delta q$ is the correlation length of the system and r is the distance to the scattering core. This assumption is in agreement with the exponentially decaying oscillation of the force measured with AFM. Thus, $2/\Delta q$ can be compared with the AFM decay length λ. The mesh size in the bulk is reciprocally related to the peak position q_{max}, i.e., $2\pi/q_{max}$, and can be compared with the force period d from the AFM force measurements.

The most important characteristic lengths of the polyelectrolyte solutions and their notations are summarized in Table 1. In the first column of Table 1, the general notations and their physical meaning are listed. In the next two columns, their corresponding expressions in film and in bulk in terms of measurable parameters are summarized. In the following sec-

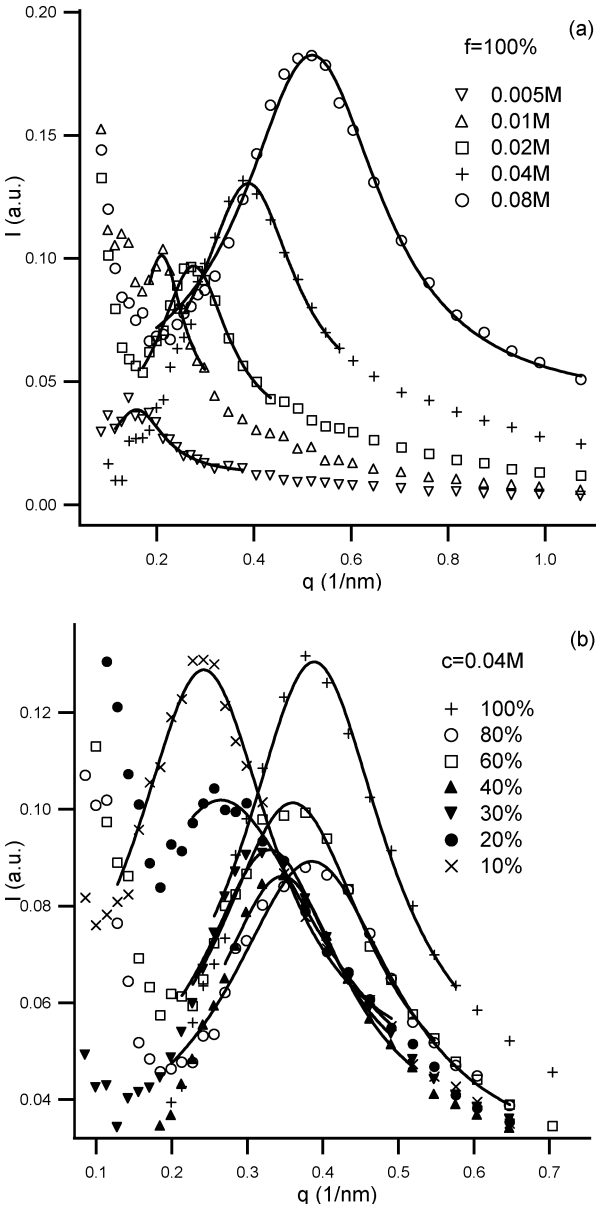

Figure 3. SAXS scattering intensity vs q vector for different sample series. (a) Sample series I with fixed charge fraction $f = 100\%$ and varying repeat unit concentration c. (b) Sample series II with fixed repeat unit concentration $c = 0.04$ M and varying charge fraction f. Data are fitted to the Lorenzian form.

Table 1. Notations of Characteristic Lengths with Their Corresponding Parameters in Film and in Bulk

characteristic length	corresponding parameter in film	corresponding parameter in bulk[a]
mesh size(ξ)	force period d	$2\pi/q_{max}$
correlation length	force decay length λ	$2/\Delta q$

[a] q_{max}: peak position; Δq: peak width.

tions, these corresponding parameters in film and in bulk will be analyzed quantitatively and compared. If there exists any effect of geometrical confinement, it shall be reflected in the change of the values from bulk to film.

III.1. AFM Force Period d and SAXS Peak Position q_{max}. Figure 4a shows the comparison between the period d measured with AFM and the inverse of the SAXS peak width $2\pi/q_{max}$ for sample series I at a fixed degree of polymer charge f of 100%. Both d and $2\pi/q_{max}$ are plotted vs c. There is a remarkable agreement between the results from the two methods, which

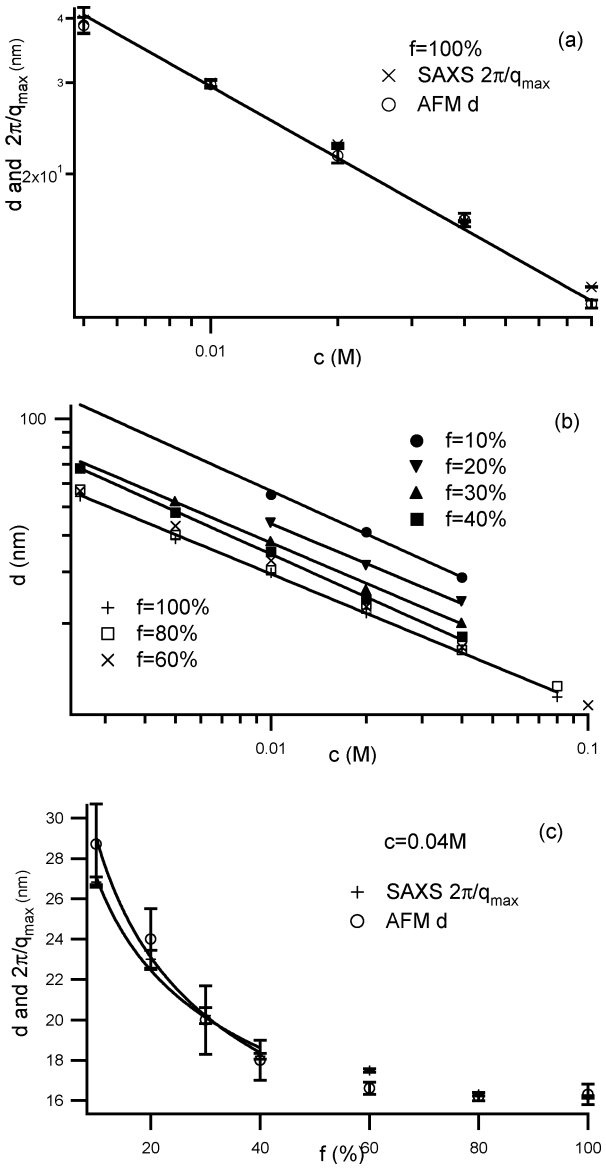

Figure 4. (a) Comparison between AFM period d and SAXS $2\pi/q_{max}$ for sample series I, varying c at fixed charge, plotted as d and $2\pi/q_{max}$ vs c in a log−log scale. Solid line: fit $d \sim c^{-1/2}$. (b) AFM period d vs repeat unit concentration c for differently charged PTRIS-*co*-AMPS solutions, plotted in a log−log scale. Solid lines: fits $d \sim c^{\alpha}$ where $\alpha \approx -1/2$ for all charge fractions. (c) Comparison between AFM period d and SAXS $2\pi/q_{max}$ for sample series II, varying charge at fixed c. Solid line: fit $d \sim f^{\gamma}$ where $\gamma = -0.27 \pm 0.02$ for the SAXS and $\gamma = -0.32 \pm 0.04$ for the AFM results.

shows $d = 2\pi/q_{max}$. Both lengths show the same $c^{-1/2}$ dependency on c.

In Figure 4b, d is plotted vs c for all different charge fractions. At each charge fraction f, the straight lines in the log−log plot indicate that d follows the power law $d \propto c^{-1/2}$ without exception, confirming the result from sample series I for the $f = 100\%$ solutions. This also reconfirms the theoretical prediction of $\xi \sim c^{-1/2}$ [1,41] and agrees with previous experimental results on hydrophilic polyelectrolytes.[5,9−12,14,15,18,20,24,42] That the power of c does not change from $-1/2$ to $-1/3$ as the charge fraction decreases indicates that, despite the increase of the average chain distance, the chain configuration in solution has not changed from a homogeneous mesh structure to one containing microdomains of coiled "pearls". This is different from the behavior of polyelectrolytes with a more hydrophobic backbones.[21,43,44] The prefix of the $d \propto c^{-1/2}$ power fit depends on f.

The curves in Figure 4b indicates that the curves for strongly charged chains ($f \geq 60\%$) are coincident, and it becomes more visible in Figure 4c, where d and $2\pi/q_{max}$ are shown vs f at a fixed concentration of 0.04 M (data series II). Two distinctly different behaviors are found for low and high degrees of charge. For $f \leq 40\%$, d increases significantly as f decreases. This behavior is predicted by theoretical models.[4] But for $f \geq 60\%$, d stays approximately constant irrespective of the degree of polymer charge. This behavior seems to support the Manning condensation theory, and the threshold charge fraction should be between 40 and 60%. The 45% value from previous experiments[37] can thus serve as a good estimation. The effective charge on the chains as well as the counterion concentration in solution should then be the same for all $f > 45\%$. This may explain why d remains almost constant when f decreases from 100 to 60%. Therefore, at distance d, the approximation by using Manning's theory for counterion condensation is valid. The chains seem to have a constant effective charge independent of the nominal charge due to the counterion condensation. The very slight increase of d for 60%, however, may be an indication that Manning's theory works less well for a border case close to the threshold charge fraction.

The relation $d = 2\pi/q_{max}$ also holds for data series II with changing f (see Figure 4c). We have fitted both d and $2\pi/q_{max}$ to the power of f. The two power fits yield 0.32 ± 0.04 and 0.27 ± 0.02, respectively, and agree with each other within the error bars. The powers also agree with the theoretical prediction of $\xi \sim f^{-2/7}$ for flexible chains without ion condensation.[4] This sets PTRIS-*co*-AMPS chains within the category of flexible chains.

III.2. AFM Decay Length λ and SAXS Peak Width Δq. As in the previous section, the AFM and SAXS comparison is first checked for sample series I. Figure 5a shows the results from sample series I, where λ and $2/\Delta q$ are plotted vs c. Both $2/\Delta q$ and λ scale as $c^{-1/2}$. There is a good agreement between $2/\Delta q$ and λ, except for $c = 0.005$ M, where the low contrast of the SAXS data makes the determination of the width unreliable (see Figure 3a). Both λ and $2/\Delta q$ describe interaction range. A smaller λ or larger Δq indicates a stronger screening of interactions, which corresponds to a more disordered structure. $\lambda = 2/\Delta q$ implies a negligible, if not nonexistent, confinement effect on the degree of ordering in the direction perpendicular to the film surface. Certainly, the exhibition of the force decay relies on the existence of confinement,[46,47] as the surfaces do rearrange the structure ordering.[48−50] However, such surface rearrangement is rather restricted in the film plane and not in the perpendicular direction and thus does not cause the lengths of either d or λ in the perpendicular direction to change.

Figure 5b shows λ vs c for all different charge fractions. The decay length λ also follows a power law of $\sim c^{-1/2}$ for all degrees of charge.

Figure 5c shows the comparison between λ and $2/\Delta q$ from sample series II. There are greater deviations here than in data series I, and λ and $2/\Delta q$ are not always in good agreement when $f \leq 40\%$, due mainly to the low contrast in the SAXS experiment, especially at $f = 20\%$ and $f = 10\%$, of which the data points are not shown in Figure 5c. However, the qualitative trend of a nonmonotonic dependence with a minimum near $f = 60\%$ is visible. Above this degree of charge, λ and $2/\Delta q$ increase with increasing f. Below $f = 60\%$, the behavior is not so clear due to large error bars. At the concentration chosen in Figure 5c, the correlation length (λ and $2/\Delta q$) is more or less independent of f. At other concentrations (see Figure 5b), there seems to be a slight increase with decreasing f, and this increase is systematic.

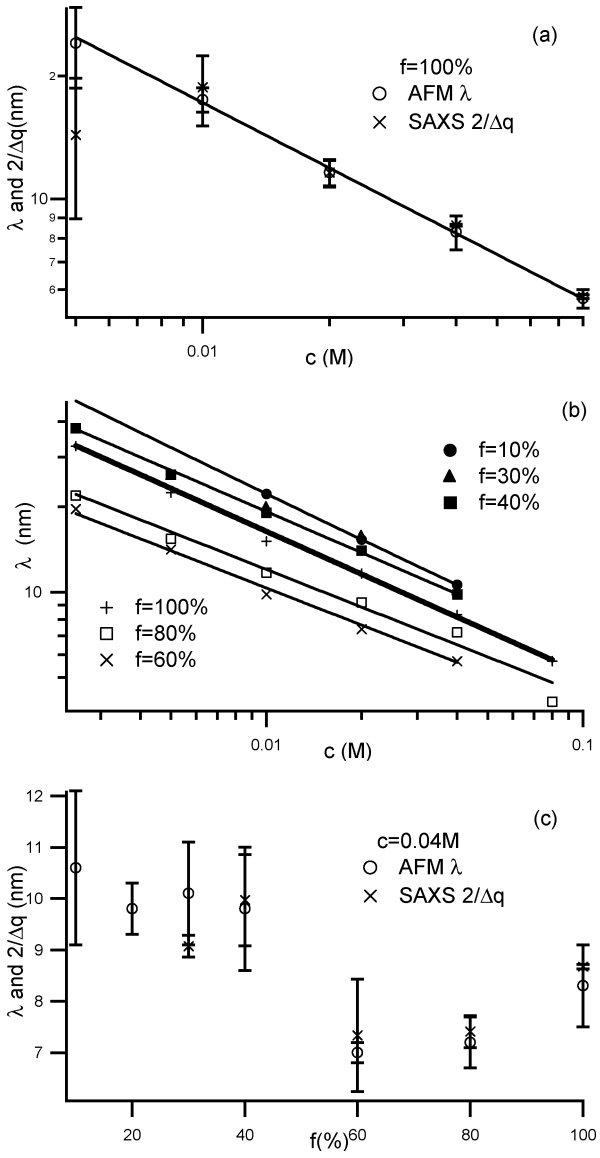

Figure 5. (a) Comparison between AFM decay length λ and SAXS correlation length $2/\Delta q$ for sample series I, varying c at fixed charge, plotted as λ and $2/\Delta q$ vs c in a log−log scale. Solid line: fit $\lambda \sim c^{\beta}$ where $\beta = -0.53 \pm 0.03$. (b) AFM decay length λ vs repeat unit concentration c for differently charged PTRIS-*co*-AMPS solutions, plotted in a log−log scale. Solid lines: fits $\lambda \sim c^{\beta}$ where $\beta \approx -1/2$ for all charge fractions. (c) Comparison between AFM decay length λ and SAXS correlation length $2/\Delta q$ for sample series II, varying charge at fixed c.

As Manning's theory of ion condensation assumes that the condensed ions completely neutralize the excess polyion charges, they should not participate in any electrostatic interaction anymore but are fixed on the chains. If Manning's theory did hold at the close-up distance λ from the chains, λ should have behaved qualitatively the same as d, i.e., being independent of the nominal charge f when above the threshold charge. Since in experiments λ always changes with f, the counterions within distance λ from the chains must condense in a different way than predicted by Manning. Figure 6 shows the schematic of a model that we propose for the ion distribution. It is worth noticing that d is always significantly greater than λ (see also Figure 7). When observed from a distance $\geq d$ from the chains, there is the same ratio between "*free*" and "*condensed*" counterions within the distance d as predicted by the Manning

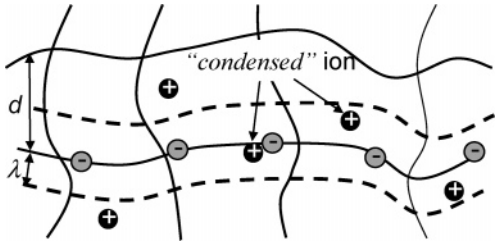

Figure 6. Schematic of the proposed model for the counterion distribution in a polyelectrolyte mesh structure.

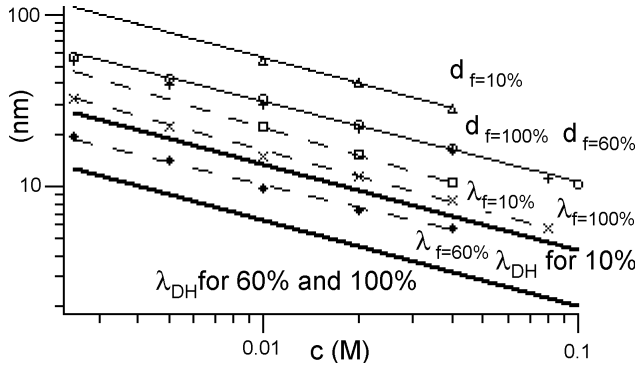

Figure 7. Comparison between the AFM period d, decay length λ, and Debye−Hückel length λ_{DH} for $f = 10$, 60, and 100%, plotted in a log−log scale.

model, and f_{eff} will remain the same for different nominal charge fractions. Therefore, the mesh size d is only influenced by f_{eff}, not by f. However, the deviation of the correlation length from Manning's model shows that a strict separation of the ions into "*free*" and "*condensed*" is not justified. On a length scale of λ or $2/\Delta q$, the Manning concept is not valid anymore. One can speculate how "*free*" and how "*condensed*" the ions are. A more plausible scheme would rather be as follows. The so-called "*condensed*" ions are not necessarily fixed on the chains, but only entrapped in a region close to the chains, forming a cloud of counterions in a manner similar to the cloud of "*free*" counterions. The extension of the counterion clouds depends on the nominal charge f. Thus, at different f, the screening of counterions will be different, causing λ to be different as well. The threshold distance at which Manning's condensation theory changes from valid to nonvalid lies somewhere between d and λ.

It is worth going into more detail regarding the correlation between the decay length and the counterion condensation. λ is reminiscent of the Debye−Hückel length λ_{DH}, which also scales as $\sim c^{-1/2}$ and characterizes the counterion screening in solution. Figure 7 shows the comparison of d, λ, and λ_{DH} for 10, 60, and 100% charged PTRIS-*co*-AMPS, in which $\lambda_{DH} = 1/\sqrt{4\pi l_B f_{eff} c}$. The Debye−Hückel length decreases with increasing f_{eff} due to a larger amount of counterion screening. Under the assumption that Manning's law of ion condensation holds, $f_{eff} = 10\%$ for $f = 10\%$ chains and $f_{eff} = 45\%$ for both $f = 60\%$ and $f = 100\%$. Accordingly, λ_{DH} for 60 and 100% charged PTRIS-*co*-AMPS are the same. Figure 7 shows that d is always greater than λ, and both are greater than λ_{DH} for all charges. Since λ_{DH} reflects the screening range of the electrostatic interaction due only to "*free*" counterions, the fact that $\lambda_{DH} < \lambda$ indicates that, with respect to the force decay, the effect of screening is somehow reduced. An explanation could be that it reflects a combined effect of "*condensed*" counterions and the polyion charges besides the "*free*" ions.[45] The combined effect of the former two makes the total screening weaker than that ascribed only by "*free*" counterions. Since the polyions act in the opposite way as the counterions, the two effects compete to determine λ. An alternative explanation is given by Dobrynin et al.,[4] where they conjectured that the longer screening length is due to the high charge density of the polyions which cannot be effectively screened by the counterions. Their prediction that the electrostatic screening length has a $c^{-1/2}$ dependency on c and is greater than λ_{DH} but smaller than the mesh size ξ also is qualitatively confirmed by our results.

In this image, all counterions are mobile below a threshold charge fraction. As f decreases, both the concentration of "*free*" ions and that of the bare polyion charges decrease. Since in Figure 5b λ increase as f decreases, the overall effect of screening is weaker at lower charges. This could suggest that the effect of counterion screening is dominating when $f \leq 40\%$. However, when $f \geq 60\%$, the effect of f on λ is opposite from that for $f \leq 40\%$. One possible explanation could be as follows: Because of the insufficient neutralization of the excess polyion charges by the "*condensed*" ions, when f increases, even the "*free*" counterions are somehow trapped by the strong polyion charges, which would effectively cause less screening and thus cause λ to increase. In other words, the price paid for the "*condensed*" ions to be mobile to a certain extent is that the "*free*" ions become less free and tend to distribute closer to the chains. And the higher the polyion charges, the higher this tendency. Therefore, for $f \geq 60\%$, the effect of polyion charges seems to dominate. This difference in whether the counterions or the polyion charges dominate might cause the different dependencies of λ on f below and above the threshold charge fraction.

III.3. AFM Amplitude. As shown in Figure 8a, for fixed charge fraction ($f = 100\%$), the amplitude is proportional to the repeat unit concentration c. As shown in Figure 8b, for fixed repeat unit concentration ($c = 0.04$ M), the amplitude is also proportional to the charge fraction f. This implies that A is proportional to the total concentration of polymer charges in the system, fc. Figure 8c shows the amplitude vs the product of f and c, which shows $A \propto fc$, with slight deviations at $c = 0.08$ M, $f = 100\%$ and $c = 0.02$ M, $f = 100\%$. fc is both the total number of polyion charges and the total number of counterions in the solution. The increase in polymer charge density leads to an increase in amplitude, while the connected increase in counterion concentration leads to a decrease in amplitude. For instance, when salt is added to the solutions, in which case the number of polyion charges remains unchanged, A decreases significantly. The outcome of this competition as shown in Figure 8c indicates clearly that polyion charge is the dominating factor that controls A. Combined with the influence of polyion charge on the decay length that has been discussed previously, we see that the polyion charge is playing an important role in the oscillatory force. It is worth noting, however, that when the concentration is very high and the charge fraction very low, the amplitude is suppressed and does not follow the nice linear laws, probably partially due to the high viscosity of the solutions.

III.4. Stiffness of the Structure. Since the slope of the force−distance curve reflects the stiffness of the structure, we can easily understand the change of stiffness with c and f by taking the derivative of $F/2\pi R$:

$$\frac{1}{2\pi R}\frac{dF}{dx} = A\sqrt{\left(\frac{1}{\lambda}\right)^2 + \left(\frac{2\pi}{d}\right)^2}\, e^{-x/\lambda} \cos\left(2\pi \frac{x}{d} + \varphi\right) \qquad (3)$$

where $\varphi = \tan^{-1}(2\pi\lambda/d)$ is a phase shift. Therefore, the stiffness is depending on all the three parameters: A, d, and λ. As c increases, both d and λ decreases and A increases; thus $A[(1/\lambda)^2 + (2\pi/d)^2]^{1/2}$ increases. Therefore, the higher the concentra-

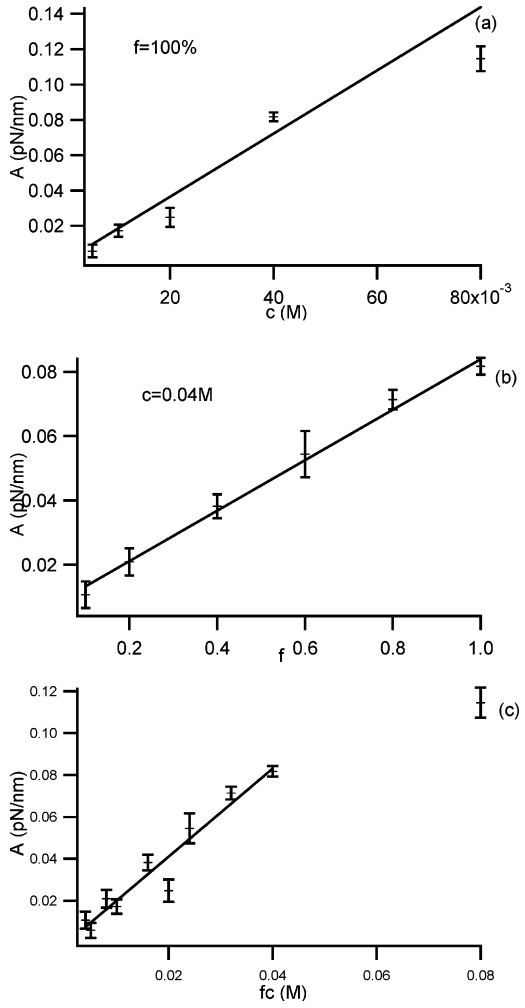

Figure 8. AFM force Amplitude plotted (a) vs repeat unit concentration c at fixed $f = 100\%$; (b) vs charge fraction f at fixed $c = 0.04$ M; (c) vs fc.

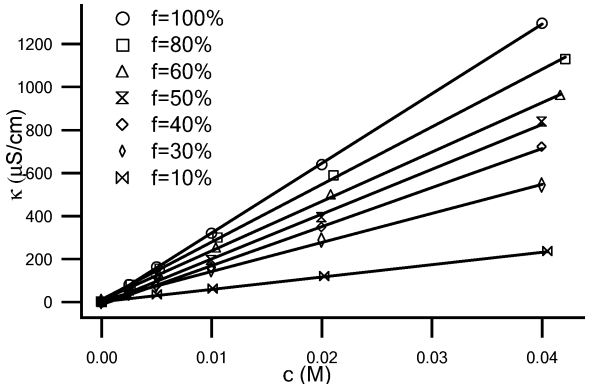

Figure 9. Conductivity κ vs repeat unit concentration c for differently charged PTRIS-*co*-AMPS.

tion, the more energy it takes to compress the film. In other words, more concentrated solutions are less compressible, as one would expect.

III.5. Conductivity and Ion Mobility. To get further understanding of the counterion distribution, the conductivity κ of each solution was measured for each charge fraction at different concentrations. The results are shown in Figure 9. For each charge fraction f, there is a constant linear dependency of κ on c, namely, $\kappa = \Lambda c$. In the case that all conducting components contribute equally to the conductivity, Λ would be the specific conductance. The fitted Λ's are listed in Table 2. We assign Λ_{Manning} to be the specific conductance of counterions when assuming Manning condensation and only free counterions conduct and Λ_{free} to be the specific conductance when assuming all counterions are free. Thus $\Lambda_{\text{Manning}} = ef_{\text{eff}}\mu_{\text{Na}^+}$ and $\Lambda_{\text{free}} = ef\mu_{\text{Na}}$, where $\mu_{\text{Na}^+} = 5.19 \times 10^{-8}$ m^2 V^{-1} s^{-1} is the mobility of free Na^+ in the limit of $c \rightarrow 0$. The values of Λ_{Manning} and Λ_{free} are also listed in Table 2.

Table 2. Fitted Λ Values from $\kappa = \Lambda c$[a]

f (%)	Λ (A m^2 V^{-1} mol^{-1})	Λ_{Manning} (A m^2 V^{-1} mol^{-1})	Λ_{free} (A m^2 V^{-1} mol^{-1})	Λ/f (A m^2 V^{-1} mol^{-1})
100	0.003 23	0.002 25	0.005 00	0.003 23
80	0.002 68	0.002 25	0.004 00	0.003 35
60	0.002 30	0.002 25	0.003 00	0.003 83
40	0.001 81	0.002 00	0.002 00	0.004 53
30	0.001 35	0.001 50	0.001 50	0.004 49
10	0.000 57	0.000 50	0.000 50	0.005 74

[a] Λ_{Manning}: the specific conductance when assuming Manning condensation and only free ions conduct; Λ_{free}: the specific conductance when assuming all counterions are free ions; and Λ/f: the average conductance for each charged ion pair.

If Manning condensation were to be understood in the way that all condensed ions are fixed on the chains and only free ions could contribute to the conductivity, one would then expect the value Λ to be independent of f for all $f > 45\%$. However, this is not the case, as shown in Table 2. In fact, for all $f \geq 60\%$, we find that the measured Λ fulfills $\Lambda_{\text{Manning}} < \Lambda < \Lambda_{\text{free}}$. Therefore, the actual total mobility of ions is between that ascribed by Manning's theory and that if all ions were free. This also supports the result from the AFM measurements of force decay length λ. Namely, the "*condensed*" ions also are mobile and contribute to conductivity. Yet, for $f = 60\%$, $\Lambda_{\text{Manning}} < \Lambda$ while for $f = 40\%$, $\Lambda_{\text{Manning}} > \Lambda$, indicating a threshold charge fraction which is fairly close to the previously observed 45% value.[37]

In addition to "*free*" and "*condensed*" ions, polyion chains could also contribute to the conductivity. Thus, a full expression of Λ should be written as $\Lambda = \sum ef_{\text{eff}}\mu_i$, where μ_i represents the mobility of all conducting components, both the conducting counterions and the polyions. To avoid the complications from the problem that "*condensed*" ions, "*free*" ions and polyions all have different mobilities, we can assign an average mobility Λ/f to each ion pair. The values of Λ/f are also listed in Table 2. It is particularly noteworthy that Λ/f increases with decreasing f, which indicates that the average mobility of each ion pair is higher at lower charges. This monotonic dependency of average ion pair mobility on f is qualitatively different from that of the force decay length λ, recalling that λ decreases with increasing f when $f \leq 40\%$ but increases when $f \geq 60\%$. When $f \leq 40\%$, their behaviors fit together into a unified picture. Namely, the charge dissociation is more complete and the polyion chains themselves are more like bare charges, causing a more ordered structure (larger λ), and each ion pair also has a higher average mobility. When $f \geq 60\%$, the situation is complicated by the different contribution from "*free*" ions, "*condensed*" ions, and polyions, and there is no direct connection between the two phenomena.

IV. Conclusion

We have studied the effect of polymer charge and geometrical confinement on the mesh structures of semidilute solutions of a typical hydrophilic polyelectrolyte. Counterion condensation plays an important role to regulate the structure and interaction in the solution. To investigate the effect of confinement, AFM results in films are compared with SAXS results in bulk. Both techniques are suitable for the determination of the characteristic

lengths of the polyelectrolyte system, i.e., mesh size and correlation length. The good agreement between the results of the two completely different methods indicates no effect of confinement on the mesh size and correlation length of the network structure in the direction perpendicular to the film plane, although the observation of the force decay is only possible under such confinement. Manning's theory for counterion condensation is valid only within a limit, i.e., beyond certain threshold distance from the polyion chains. The mesh size is beyond this threshold distance and is thus not influenced by the charge fraction so long as the effective charge fraction as predicted by Manning's theory remains constant. However, the structure ordering of the system is reflected in the decay length of the force oscillation, which is smaller than this threshold distance where Manning's theory no longer holds. The force decay thus reveals finer structures at the vicinity of polyion chains, namely, the "*condensed*" ions are actually mobile and form a counterion cloud in the close vicinity of the chains. This idea is further supported by evidence from conductivity measurements, where the "*condensed*" ions seem also to contribute to the conductivity.

Acknowledgment. The authors express their gratitude to A. Fery for help in introducing the AFM technique, R. Netz and D. Langevin for helpful discussions, and G. Roshan Deen for assistance with some of the SAXS measurements and to the financial support of the French-Germany network "Complex fluids: from 3D to 2D" and the RTN European Network SOCON.

References and Notes

(1) De Gennes, P.-G.; Pincus, P.; Velasco, R. M.; Brochard, F. *J. Phys. (Paris)* **1976**, *37*, 1461−1473.
(2) Odijk, T. *J. Polym. Sci., Polym. Phys. Ed.* **1977**, *15*, 477−483.
(3) Skolnick, J.; Fixman, M. *Macromolecules* **1977**, *10*, 944−948.
(4) Dobrynin, A. V.; Colby, R. H.; Rubinstein, M. *Macromolecules* **1995**, *28*, 1859−1871.
(5) Nierlich, M.; Williams, C. E.; et al. *J. Phys. (Paris)* **1979**, *40*, 701−704.
(6) Williams, C. E.; Nierlich, M.; et al. *J. Phys. Sci., Polym. Lett. Ed.* **1979**, *17*, 379.
(7) Nierlich, M.; Boué, F.; Lapp, A.; Oberthür, R. *J. Phys. (Paris)* **1985**, *46*, 649−655.
(8) Nierlich, M.; Boué, F.; Lapp, A.; Oberthür, R. *Colloid Polym. Sci.* **1985**, *263*, 955−964.
(9) Essafi, W.; Lafuma, F.; Williams, C. E. *Eur. Phys. J. B* **1995**, *9*, 261−266.
(10) Nishida, K.; Kaji, K.; Kanaya, T. *Macromolecules* **1995**, *28*, 2472−2475.
(11) Klitzing, R. v.; Kolaric, B.; Jaeger, W.; Brandt, A. *Phys. Chem. Chem. Phys.* **2002**, *4*, 1907−1914.
(12) Klitzing, R. v.; Espert, A.; Asnacious, A.; Hellweg, T.; Colin, A.; Langevin, D. *Colloids Surf., A.* **1999**, *149*, 131−140.
(13) Bergeron, V.; Langevin, D.; Asnacios, A. *Langmuir* **1996**, *12*, 1550−1556.
(14) Asnacios, A.; Espert, A.; Collin, A.; Langevin, D. *Phys. Rev. Lett.* **1997**, *78*, 4974−4977.
(15) Kolaric, B.; Jaeger, W.; Klitzing, R. v. *J. Phys. Chem. B* **2000**, *104*, 5096−5101.
(16) Klitzing, R. v.; Müller, H.-J. *Curr. Opin. Colloid Interface Sci.* **2002**, *7*, 18−25.
(17) Stubenrauch, C.; Klitzing, R. v. *J. Phys.: Condens. Matter* **2003**, *15*, R1197−R1232.
(18) Milling, A. J. *J. Phys. Chem.* **1996**, *100*, 8986−8993.
(19) Milling, A. J.; Vincent, B. *J. Chem. Soc., Faraday Trans.* **1997**, *93*, 3179−3183.
(20) Kendall, K.; Milling, A. J. *Langmuir* **2000**, *16*, 5106−5115.
(21) Qu, D.; Baigl, D.; Williams, C. E.; Möhwald, H.; Fery, A. *Macromolecules* **2003**, *60*, 6878−6883.
(22) Piech, M.; Walz, J. Y. *J. Phys. Chem. B* **2004**, *108*, 9177−9188.
(23) Klitzing, R. v. *Tenside, Surfactants. Deterg.* **2000**, *37*, 338−345.
(24) Théodoly, O.; Tan, J. S.; Ober, R.; Williams, C. E.; Bergeron, V. *Langmuir* **2001**, *17*, 4910−4918.
(25) Moussaid, A.; Candau, S. J.; Joosten, J. G. *Macromolecules* **1994**, *27*, 2102−2110.
(26) Manning, G. S. *J. Chem. Phys.* **1969**, *51*, 924−933.
(27) Oosawa, F. *Polyelectrolytes*; Marcel Dekker: New York, 1971.
(28) Ray, J.; Manning, G. S. *Macromolecules* **1997**, *30*, 5739−5744.
(29) Olvera de la Cruz, M.; Belloni, L.; Delsanti, M.; Dalbiez, J. P.; Spalla, O.; Drifford, M. *J. Chem. Phys.* **1995**, *103*, 5781−5791.
(30) Wilson, R. W.; Bloomfield, V. A. *Biochemistry* **1979**, *18*, 2192−2196.
(31) Bloomfield, V. A. *Biopolymers* **1997**, *44*, 269−282.
(32) Raspaud, E.; Olvera de la Cruz, M.; Sikorav, J.-L.; Livolant, F. *Biophys. J.* **1998**, *74*, 381−393.
(33) Yamasaki, Y.; Teramoto, Y.; Yosjikawa, K. *Biophys. J.* **2001**, *80*, 2823−2832.
(34) Netz, R. R. *J. Phys. Chem. B* **2003**, *107*, 8208−8217.
(35) Manghi, M.; Netz, R. R. *Eur. Phys. J. E* **2004**, *14*, 67−77.
(36) Delorme, N.; Dubois, M.; Garnier, S.; Laschewsky, A.; Weinkamer, R.; Zemb, T.; Fery, A. *J. Phys. Chem. B* **2006**, *110*, 1752−1758.
(37) Essafi, W. Ph.D. Thesis, Paris VI France, 1996.
(38) Ducker, W. A.; Senden, T. J.; Pashley, R. M. *Nature (London)* **1991**, *353*, 239−241.
(39) Riegler, H.; Engel, M. *Ber. Bunsen-Ges. Phys. Chem.* **1991**, *95*, 1424−1430.
(40) Pedersen, J. S. *J. Appl. Crystallogr.* **2004**, *37*, 369−380.
(41) Odijk, T. *Macromolecules* **1979**, *12*, 688−693.
(42) Förster, S.; Schmidt, M. *Adv. Polym. Sci.* **1995**, *120*, 51−133.
(43) Dobrynin, A. V.; Rubinstein, M. *Macromolecules* **1999**, *32*, 915−922.
(44) Limbach, H. J.; Holm, C.; Kremer, K. *Europhys. Lett.* **2002**, *60*, 566−572.
(45) Châtllier, X.; Joanny, J.-F. *J. Phys. II* **1996**, *6*, 1669−1686.
(46) Israelachvili, J. *Intermolecular & Surface Forces*; Academic Press Limited: London, 1992; Chapter 13, p 260.
(47) Yethiraj, A. *J. Chem. Phys.* **1999**, *111*, 1797−1800.
(48) Rapoport, D. H.; Anghel, A. F.; Handike, G.; Möhwald, H.; Klitzing, R. v., submitted to *J. Am. Chem. Soc.*
(49) Colby, R. H.; Boris, D. C.; Krause, W. E.; Tan, J. S. *J. Polym. Sci.* **1997**, *35*, 2951−2960.
(50) Muthukumar, M. *Macromol. Theory Simul.* **1994**, *3*, 61−71.

MA052676Q